ACS Energy LETTERS

http://pubs.acs.org/journal/aelccp

Inhomogeneous Defect Distribution in Mixed-Polytype Metal Halide Perovskites

Young Won Woo, Zhenzhu Li, Young-Kwang Jung, Ji-Sang Park, and Aron Walsh*

Cite This: *ACS Energy Lett.* 2023, 8, 356−360

Read Online

ACCESS | Metrics & More | Article Recommendations | Supporting Information

ABSTRACT: **The competition between corner-, edge-, and face-sharing octahedral networks is a cause of phase inhomogeneity in metal halide perovskite thin-films. Here we probe the charged iodine vacancy distribution and transport at the junction between cubic and hexagonal polytypes of $CsPbI_3$ from first-principles materials modeling. We predict a lower defect formation energy in the face-sharing regions, which correlates with a longer Pb−I bond length and causes a million-fold increase in local defect concentration. These defects are predicted to be more mobile in the face-sharing regions with a reduced activation energy for vacancy-mediated diffusion. We conclude that hexagonal phase inclusions or interfaces will act as defect sinks that could influence carrier dynamics in perovskite-based solar cells and electrical devices.**

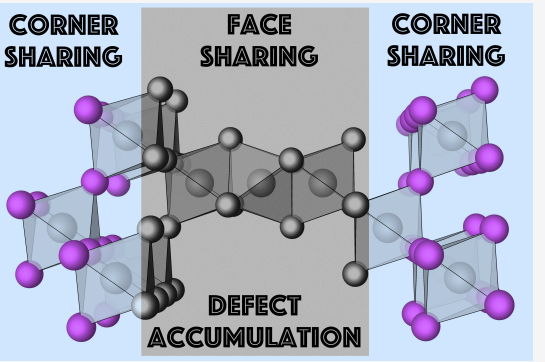

Metal halide perovskites are promising materials for photovoltaic and optoelectronic applications.[1] Single-junction metal halide perovskite solar cells have achieved power conversion efficiencies of more than 25% in just over a decade since their first report.[2−5] However, structural transformations from photoactive corner-sharing phases (e.g., cubic or tetragonal) to photoinactive edge- or face-sharing phases are a cause of degradation.[6−8] Beyond simple phase mixing, a range of ordered polytype structures can be formed.[9−12] Interesting phenomena can emerge at the interface between regions of different connectivity.[13−15] For example, fast ion diffusion has been observed between corner- and face-sharing regions of 6H metal oxide polytype derivatives, which is linked to a high concentration of defects.[16]

There is increasing evidence that hexagonal phase inclusions are ubiquitous in metal halide perovskite films, even those with high photovoltaic performance.[15,17] For example, the presence of 2H polytype domains has been associated with high photocarrier trap concentrations from photoemission electron microscopy.[18] The growing consensus is that domains of such secondary phases can generate clusters of sub-bandgap states, centered 1 eV below the Fermi level,[19] that trap photoexcited carriers and cause recombination that is detrimental to photovoltaic performance.[7,20−22] Polytype defect clustershave been found to be less detrimental than grain boundary defect clusters in perovskite thin-films;[19] but they can significantly impact the overall film performance as their abundance increases. However, the underlying origin and mechanism for such behavior have not been identified.

In this work, we report an investigation of the charged halide vacancy distribution and transport at the interface between corner- and face-sharing regions of $CsPbI_3$ using first-principles materials simulations. We model the defect processes using a representative 11H polytype that consists of two face-sharing layers ($2h$) connected to nine corner-sharing layers ($9c$) as shown in Figure 1a. For comparison, results for the alternative 11H $3c8h$ polytype are included as Supporting Information. We demonstrate that hexagonal phase inclusions or interfaces act as defect sinks in metal halide perovskites with mobile anion vacancy defects.

Defect Accumulation at Interfacial and Face-Sharing Regions. The optimized crystal structures for the 11H polytypes of $CsPbI_3$ were taken from a previous study on the bulk crystal properties.[12] To describe the formation of point defects, a supercell expansion of 2 × 2 × 1 formed of 220 atoms was used. We identified all symmetry inequivalent iodine vacancy sites (V_I^+) to reduce the complexity of the problem to just six distinct defect types. As this is the stable charge state of the iodine vacancy across a wide Fermi level range, there is no dependence on the electronic chemical potential. The associated defect formation energies were then

Received: October 12, 2022
Accepted: November 30, 2022
Published: December 6, 2022

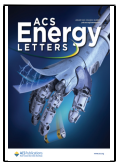

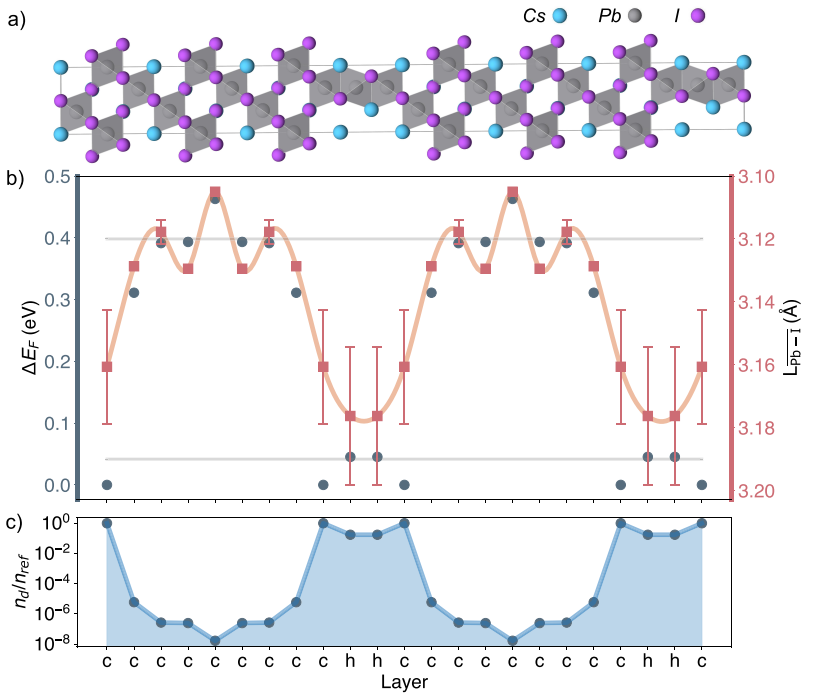

Figure 1. (a) Illustration of the 11H ($2h9c$) polytype structure of $CsPbI_3$. The lead iodide octahedra are shaded gray. Note that the stacking axis corresponds to the ⟨111⟩ direction for a cubic perovskite unit cell. (b) Relative defect formation energy (ΔE_F, blue dots) and average Pb−I length ($\Delta L_{\overline{Pb-I}}$, red squares) along the stacking layers. The gray horizontal lines represent the average Pb−I bond length in the perfect cubic (3.12 Å) and hexagonal (3.19 Å) structures. The error bars denote the deviation from the average Pb−I length in each octahedron; the curved line is drawn to guide the eye. (c) Relative defect concentration assuming thermodynamic equilibrium at T = 300 K.

combined to reconstruct the full energy landscape plotted in Figure 1.

The computed V_I^+ formation energies in the $2h9c$ structure are shown in Figure 1b. To avoid setting an atomic chemical potential for iodine, which requires consideration of the specific processing conditions and chemical environment that may involve gas, solid, or liquid exchanges with the perovskite crystal, we set the lowest energy configuration to zero and compared the relative defect formation energies. A spread of 0.5 eV is found for forming the same defect type in different coordination environments. A clear two-region behavior is observed in the formation energies with a higher-energy group in the corner-sharing regions and a lower-energy group in the face-sharing regions. An underlying correlation is found between the V_I^+ defect formation energy and the Pb−I bond length. The corner-sharing regions have bond lengths similar to those in the parent 3C cubic perovskite (∼3.12 Å), while the face-sharing regions have shorter bond lengths similar to the parent 2H phase (∼3.19 Å). Iodine vacancy formation is preferred in the regions of the polytype with bond elongation.

To understand the impact of the defect formation energies on the iodine vacancy defect distributions, the equilibrium concentrations were then calculated. The absolute concentration for a single defect species (n_d) is defined by the standard equilibrium expression

$$n_d = N_{site} \exp\left(-\frac{\Delta E_F}{k_B T}\right) \quad (1)$$

where N_{site} represents the number of available crystal sites, ΔE_F is the defect formation energy, k_B is the Boltzmann constant, and T is temperature.[23] We define the relative defect concentration (n_d/n_{ref}) as

$$\frac{n_d}{n_{ref}} = \exp\left(-\frac{\Delta E_F - \Delta E_{ref}}{k_B T}\right) \quad (2)$$

where n_{ref} refers to the concentration at the site with lowest formation energy ΔE_{ref}. The distributions are plotted in Figure 1c, which highlight fluctuations over many orders of magnitude. A high vacancy concentration is found around the face-sharing region, which is ∼10^6 times higher than the plateau in the corner-sharing region due to the exponential dependence on the underlying formation energy. The highest overall concentration is found in the interfacial layer, which is strained with bond length values that are shorter than the face-sharing regions and longer than the corner-sharing regions. Based on these results, we conclude that hexagonal phase inclusions or interfaces are likely to act as sinks for vacancy defects in halide perovskites. The predictions are consistent with the recent report by Macpherson et al.[18] that highlighted the high concentration of structural defects at the polytype junction, consistent with vacancies, which degrade device performance.

Microscopic Origin of the V_I^+ Defect Distribution. Strain is an important parameter in the property control of metal halide perovskites. It is an intrinsic feature of perovskite-derived polytypes owing to the combination of building blocks with differing connectivity in the same crystal.[21] In particular, large changes in Pb−I bond lengths are found along the stacking axis of mixed polytypes. The lowest defect formation energy is calculated at the stacking interface with expanded cubic and compressed hexagonal layers. For the case of homogeneous hydrostatic strain in a purely corner-sharing perovskite, lattice expansion makes iodine vacancy formation less favorable.[24] The behavior is different here as the strain is nonuniform with an elastic dipole centered around the

https://doi.org/10.1021/acsenergylett.2c02306
ACS Energy Lett. 2023, 8, 356−360

interfacial iodide layer that reduces the defect formation energy.

Another factor that contributes to the vacancy formation energy is the underlying atomic rearrangements upon defect formation. After removing an I^- ion from the crystal, the electrostatic balance in the $Pb^{2+}-I^-Pb^{2+}$ units along the stacking axis is replaced by a repulsive $Pb^{2+}-V_I^+-Pb^{2+}$ interaction, which will force the pair of Pb^{2+} cations in neighboring octahedra away from each other, leading to elongated Pb−Pb distances. The corresponding change in Pb separation is shown in Figure 2. In both cubic and hexagonal

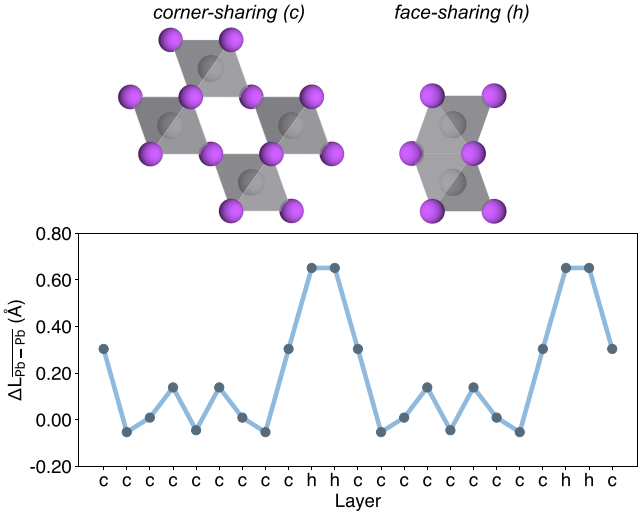

Figure 2. Pb−Pb bond length changes ($\Delta L_{\overline{Pb-Pb}}$, blue dots) following structural relaxation with a positively charged iodine defect and the pristine structure of the 11H (2*h*9*c*) polytype.

regions, elongated Pb−Pb distances were found; however, the magnitude of the change in the hexagonal layers is larger and exceeds 0.6 Å, whereas the change in the cubic layers is less than 0.1 Å. In the interface region, an elongated Pb−Pb distance of 6.62 Å (from 6.31 Å) was observed with a 0.3 Å displacement of the Pb atoms. The correlation between the larger bond elongation in Figure 2 and lower defect formation energy in Figure 1b indicates a stabilization in the face-sharing regions that is likely driven by enhanced structural relaxation and the associated electrostatic stabilization.

Charged Vacancy Transport. It is now well established that defects in metal halide perovskites are mobile, in particular on the anion sublattice.[25−28] The magnitude of ionic transport depends on the concentration of diffusing species and their activation energy, in addition to external factors such as light exposure and applied electric fields.[29−31]

We first compare the calculated ion migration barrier in the face-sharing (2H) and corner-sharing (3C) structures. A transition state search is performed using the nudged elastic band (NEB) method,[32] with a climbing-image algorithm based on five images to estimate the diffusion barriers. The barrier is isotropic in the 3C phase, but there is the possibility for in-plane and out-of-plane transport in the 2H phase (see Figure 3). The calculated activation energy of 0.34 eV (3C) decreases to 0.29 eV (2H) for migrating out-of-plane along the ⟨0001⟩ stacking axis. This suggests that the face-sharing domains can support similarly high levels of ion transport. In contrast, the in-plane 2H barrier increases to 0.45 eV along ⟨1000⟩ due to

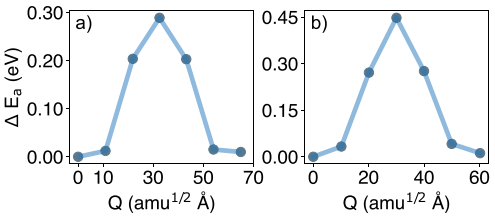

Figure 3. Calculated migration barrier (ΔE_a) for V_I^+ migration out-of-plane (a) and in-plane (b) in the hexagonal 2H phase of $CsPbI_3$. The corresponding barrier in the 3C phase is 0.34 eV at the same level of theory.

the longer separation between the face-sharing octahedral pillars.

Mechanical stress and strain affect defect mobility, and the energy barrier of halide ion migration increases with compression (applied pressure).[29,33] Therefore, at the interface with the 11H polytype, the ion migration barrier will be lowered due to the elongated Pb−I bond length (from 3.12 to 3.16 Å) in the expanded cubic region. The high defect concentration at the junction will also support a higher ion flux. We noted that our calculated energy barriers for diffusion are in good general agreement with experimental measurements, which is typically in the 0.2−0.5 eV range for vacancy-assisted halide ion diffusion in metal halide perovskites.[34]

In conclusion, we have demonstrated that hexagonal phase inclusions in metal halide perovskites will act as vacancy sinks due to a reduced formation energy in both the face-sharing regions and the interfaces between regions of different connectivity. We expect this behavior to be general for other choices of A-site cation such as methylammonium or formamidinium. The behavior is linked to changes in the Pb−I bond lengths, which show a clear correlation to the energy cost to generate the vacancy defect along the two-region polytype. The associated equilibrium distribution of defects changes by orders of magnitude. Finally, we show that the face-sharing units have comparable activation energy for defect transport compared to the regular corner-sharing perovskites.

Our study provides insights into observed behavior of these materials and opens questions for further study. First, we have established the preference for vacancy defects that are associated with current−voltage hysteresis and linked to device operational stability. However, many other defect species may also form such as isolated and aggregated halide interstitials.[35] It is becoming clear that nonradiative pathways that impact device efficiency exist at the polytype junctions,[18−20,22] but the exact combination of dilute or aggregated impurities remains to be identified. Also our current model describes the equilibrium distributions of non-interacting point defects in the dark. Illumination may change the observed behavior, including the generation of metastable defect configurations and nonequilibrium defect distributions driven by chemical potential changes. Deeper research on polytype interface stability, including the role of chemical composition, is required to complete our understanding of their role in perovskite solar cells.

METHODS

The crystals structures were generated using the POLYTYPE code available from https://github.com/WMD-group/polytype. The preprocessing and symmetry analysis for the

https://doi.org/10.1021/acsenergylett.2c02306
ACS Energy Lett. 2023, 8, 356−360

defect calculations was performed using PYMATGEN (https://pymatgen.org) and the DOPED code available from https://github.com/SMTG-UCL/doped.

The first-principles total energy and forces were obtained from Kohn–Sham density-functional theory[36,37] as implemented in VASP.[38,39] The projector augmented-wave method[40] was employed with the Perdew–Burke–Ernzerhof exchange-correlation functional revised for solids (PBEsol)[41] including scalar-relativistic effects. For all calculations, the plane-wave kinetic energy cutoff was set to 500 eV, while convergence criteria of 10^{-5} eV and 10^{-2} eV Å^{-1} for total energy and forces on each atom, respectively, were employed. For Brillouin zone sampling, Γ-centered *k*-point meshes were set to 6 × 6 × 2 and 3× 3 × 2 for geometry optimization with primitive unit cells and supercells, respectively. For the charged defect calculations, anisotropic finite-sized corrections were included following Kumagai and Oba,[42] as detailed in the Supporting Information.

■ ASSOCIATED CONTENT

Data Availability Statement

Data produced during this work is freely available in a repository at https://doi.org/10.5281/zenodo.7123720.

Supporting Information

The Supporting Information is available free of charge at https://pubs.acs.org/doi/10.1021/acsenergylett.2c02306.

Additional details on the defect correction scheme, dielectric constants, and comparable analysis for the alternative 11H (3*c*8*h*) polymorph (PDF)

■ AUTHOR INFORMATION

Corresponding Author

Aron Walsh − *Department of Materials, Imperial College London, London SW7 2AZ, United Kingdom; Department of Physics, Ewha Womans University, Seoul 03760, Korea;* orcid.org/0000-0001-5460-7033; Email: a.walsh@imperial.ac.uk

Authors

Young Won Woo − *Department of Materials, Imperial College London, London SW7 2AZ, United Kingdom; Department of Materials Science and Engineering, Yonsei University, Seoul 03722, Korea*

Zhenzhu Li − *Department of Materials, Imperial College London, London SW7 2AZ, United Kingdom;* orcid.org/0000-0002-6669-563X

Young-Kwang Jung − *Department of Chemical Engineering and Biotechnology, University of Cambridge, Cambridge CB3 0AS, United Kingdom;* orcid.org/0000-0003-3848-8163

Ji-Sang Park − *SKKU Advanced Institute of Nanotechnology and Department of Nano Engineering, Sungkyunkwan University, Suwon 16419, Korea*

Complete contact information is available at: https://pubs.acs.org/10.1021/acsenergylett.2c02306

Author Contributions

The author contributions have been defined following the CRediT system. Y.W.W.: Conceptualization, Investigation, Formal analysis, Methodology, Visualization, Writing–original draft. Z.L.: Methodology, Formal analysis, Writing–review and editing. Y-K.J.: Methodology, Writing–review and editing. J-S.P.: Methodology, Supervision, Writing–review and editing. A.W.: Conceptualization, Methodology, Supervision, Writing–review and editing.

Notes

The authors declare no competing financial interest.

■ ACKNOWLEDGMENTS

This research was supported by a grant of the Korea Health Technology R&D Project through the Korea Health Industry Development Institute (KHIDI), funded by the Ministry of Health & Welfare, Republic of Korea (grant number: HI19C1344). Computational resources have been provided by the KISTI Supercomputing Center (KSC-2021-CRE-0510). We are also grateful to the UK Materials and Molecular Modelling Hub for computational resources, which is partially funded by EPSRC (EP/P020194/1 and EP/T022213/1).

■ REFERENCES

(1) Kim, J. Y.; Lee, J.-W.; Jung, H. S.; Shin, H.; Park, N.-G. High-efficiency perovskite solar cells. *Chem. Rev.* **2020**, *120*, 7867–7918.

(2) Kojima, A.; Teshima, K.; Shirai, Y.; Miyasaka, T. Organometal halide perovskites as visible-light sensitizers for photovoltaic cells. *J. Am. Chem. Soc.* **2009**, *131*, 6050–6051.

(3) Yang, W. S.; Noh, J. H.; Jeon, N. J.; Kim, Y. C.; Ryu, S.; Seo, J.; Seok, S. I. High-performance photovoltaic perovskite layers fabricated through intramolecular exchange. *Science* **2015**, *348*, 1234–1237.

(4) Min, H.; Kim, M.; Lee, S.-U.; Kim, H.; Kim, G.; Choi, K.; Lee, J. H.; Seok, S. I. Efficient, stable solar cells by using inherent bandgap of α-phase formamidinium lead iodide. *Science* **2019**, *366*, 749–753.

(5) NREL. *Best Research-Cell Efficiencies*. https://www.nrel.gov/pv/cell-efficiency.html (accessed November 25, 2022).

(6) Stoumpos, C. C.; Malliakas, C. D.; Kanatzidis, M. G. Semiconducting tin and lead iodide perovskites with organic cations: phase transitions, high mobilities, and near-infrared photoluminescent properties. *Inorg. Chem.* **2013**, *52*, 9019–9038.

(7) Tan, S.; Yavuz, I.; Weber, M. H.; Huang, T.; Chen, C.-H.; Wang, R.; Wang, H.-C.; Ko, J. H.; Nuryyeva, S.; Xue, J.; et al. Shallow iodine defects accelerate the degradation of α-phase formamidinium perovskite. *Joule* **2020**, *4*, 2426–2442.

(8) An, Y.; Hidalgo, J.; Perini, C. A. R.; Castro-Mendez, A.-F.; Vagott, J. N.; Bairley, K.; Wang, S.; Li, X.; Correa-Baena, J.-P. Structural stability of formamidinium-and cesium-based halide perovskites. *ACS Energy Letters* **2021**, *6*, 1942–1969.

(9) Stoumpos, C. C.; Mao, L.; Malliakas, C. D.; Kanatzidis, M. G. Structure–band gap relationships in hexagonal polytypes and low-dimensional structures of hybrid tin iodide perovskites. *Inorg. Chem.* **2017**, *56*, 56–73.

(10) Park, J.-S.; Li, Z.; Wilson, J. N.; Yin, W.-J.; Walsh, A. Hexagonal stacking faults act as hole-blocking layers in lead halide perovskites. *ACS Energy Letters* **2020**, *5*, 2231–2233.

(11) Tian, J.; Cordes, D. B.; Slawin, A. M.; Zysman-Colman, E.; Morrison, F. D. Progressive polytypism and bandgap tuning in azetidinium lead halide perovskites. *Inorg. Chem.* **2021**, *60*, 12247–12254.

(12) Li, Z.; Park, J.-S.; Walsh, A. Evolutionary exploration of polytypism in lead halide perovskites. *Chemical Science* **2021**, *12*, 12165–12173.

(13) Pavlovetc, I. M.; Brennan, M. C.; Draguta, S.; Ruth, A.; Moot, T.; Christians, J. A.; Aleshire, K.; Harvey, S. P.; Toso, S.; Nanayakkara, S. U.; et al. Suppressing cation migration in triple-cation lead halide perovskites. *ACS Energy Letters* **2020**, *5*, 2802–2810.

(14) Fop, S.; McCombie, K. S.; Wildman, E. J.; Skakle, J.; Irvine, J. T.; Connor, P. A.; Savaniu, C.; Ritter, C.; Mclaughlin, A. C. High oxide ion and proton conductivity in a disordered hexagonal perovskite. *Nat. Mater.* **2020**, *19*, 752–757.

(15) Li, W.; Rothmann, M. U.; Zhu, Y.; Chen, W.; Yang, C.; Yuan, Y.; Choo, Y. Y.; Wen, X.; Cheng, Y.-B.; Bach, U.; et al. The critical

role of composition-dependent intragrain planar defects in the performance of $MA_{1-x}FA_xPbI_3$ perovskite solar cells. *Nature Energy* **2021**, *6*, 624−632.
(16) Sinclair, D. C.; Skakle, J. M.; Morrison, F. D.; Smith, R. I.; Beales, T. P. Structure and electrical properties of oxygen-deficient hexagonal $BaTiO_3$. *J. Mater. Chem.* **1999**, *9*, 1327−1331.
(17) Marchezi, P. E.; Therézio, E. M.; Szostak, R.; Loureiro, H. C.; Bruening, K.; Gold-Parker, A.; Melo, M. A.; Tassone, C. J.; Tolentino, H. C.; Toney, M. F.; et al. Degradation mechanisms in mixed-cation and mixed-halide $Cs_xFA_{1-x}Pb(Br_yI_{1-y})_3$ perovskite films under ambient conditions. *Journal of Materials Chemistry A* **2020**, *8*, 9302−9312.
(18) Macpherson, S.; Doherty, T. A.; Winchester, A. J.; Kosar, S.; Johnstone, D. N.; Chiang, Y.-H.; Galkowski, K.; Anaya, M.; Frohna, K.; Iqbal, A. N.; et al. Local nanoscale phase impurities are degradation sites in halide perovskites. *Nature* **2022**, *607*, 294−300.
(19) Kosar, S.; Winchester, A. J.; Doherty, T. A.; Macpherson, S.; Petoukhoff, C. E.; Frohna, K.; Anaya, M.; Chan, N. S.; Madéo, J.; Man, M. K.; et al. Unraveling the varied nature and roles of defects in hybrid halide perovskites with time-resolved photoemission electron microscopy. *Energy Environ. Sci.* **2021**, *14*, 6320−6328.
(20) Nan, Z.-A.; Chen, L.; Liu, Q.; Wang, S.- H.; Chen, Z.-X.; Kang, S.-Y.; Ji, J.-B.; Tan, Y.-Y.; Hui, Y.; Yan, J.-W.; et al. Revealing phase evolution mechanism for stabilizing formamidinium-based lead halide perovskites by a key intermediate phase. *Chem.* **2021**, *7*, 2513−2526.
(21) Jones, T. W.; Osherov, A.; Alsari, M.; Sponseller, M.; Duck, B. C.; Jung, Y.-K.; Settens, C.; Niroui, F.; Brenes, R.; Stan, C. V.; et al. Lattice strain causes non-radiative losses in halide perovskites. *Energy Environ. Sci.* **2019**, *12*, 596−606.
(22) Doherty, T. A.; Winchester, A. J.; Macpherson, S.; Johnstone, D. N.; Pareek, V.; Tennyson, E. M.; Kosar, S.; Kosasih, F. U.; Anaya, M.; Abdi-Jalebi, M.; et al. Performance-limiting nanoscale trap clusters at grain junctions in halide perovskites. *Nature* **2020**, *580*, 360−366.
(23) Kim, S.; Hood, S. N.; Park, J.-S.; Whalley, L. D.; Walsh, A. Quick-start guide for first-principles modelling of point defects in crystalline materials. *Journal of Physics: Energy* **2020**, *2*, 036001.
(24) Jung, Y.-K.; Abdulla, M.; Friend, R. H.; Stranks, S. D.; Walsh, A. Pressure-induced non-radiative losses in halide perovskite light-emitting diodes. *Journal of Materials Chemistry C* **2022**, *10*, 12560−12568.
(25) Eames, C.; Frost, J. M.; Barnes, P. R.; O'Regan, B. C.; Walsh, A.; Islam, M. S. Ionic transport in hybrid lead iodide perovskite solar cells. *Nat. Commun.* **2015**, *6*, 7497.
(26) Azpiroz, J. M.; Mosconi, E.; Bisquert, J.; De Angelis, F. Defect migration in methylammonium lead iodide and its role in perovskite solar cell operation. *Energy Environ. Sci.* **2015**, *8*, 2118−2127.
(27) Haruyama, J.; Sodeyama, K.; Han, L.; Tateyama, Y. First-principles study of ion diffusion in perovskite solar cell sensitizers. *J. Am. Chem. Soc.* **2015**, *137*, 10048−10051.
(28) Yang, J.-H.; Yin, W.-J.; Park, J.-S.; Wei, S.-H. Fast self-diffusion of ions in $CH_3NH_3PbI_3$: the interstiticaly mechanism versus vacancy-assisted mechanism. *Journal of Materials Chemistry A* **2016**, *4*, 13105−13112.
(29) Woo, Y. W.; Jung, Y.-K.; Kim, G. Y.; Kim, S.; Walsh, A. Factors influencing halide vacancy transport in perovskite solar cells. *Discover Materials* **2022**, *2*, 8.
(30) Walsh, A.; Stranks, S. D. Taking control of ion transport in halide perovskite solar cells. *ACS Energy Letters* **2018**, *3*, 1983−1990.
(31) Kim, G. Y.; Senocrate, A.; Yang, T.-Y.; Gregori, G.; Grätzel, M.; Maier, J. Large tunable photoeffect on ion conduction in halide perovskites and implications for photodecomposition. *Nat. Mater.* **2018**, *17*, 445−449.
(32) Mills, G.; Jónsson, H.; Schenter, G. K. Reversible work transition state theory: application to dissociative adsorption of hydrogen. *Surf. Sci.* **1995**, *324*, 305−337.
(33) Muscarella, L. A.; Hutter, E. M.; Wittmann, F.; Woo, Y. W.; Jung, Y.-K.; McGovern, L.; Versluis, J.; Walsh, A.; Bakker, H. J.; Ehrler, B. Lattice compression increases the activation barrier for phase segregation in mixed-halide perovskites. *ACS Energy Letters* **2020**, *5*, 3152−3158.
(34) Iwahara, H.*Perovskite Oxide for Solid Oxide Fuel Cells*; Springer, 2009; pp 45−63.
(35) Ambrosio, F.; Mosconi, E.; Alasmari, A. A.; Alasmary, F. A.; Meggiolaro, D.; De Angelis, F. Formation of color centers in lead iodide perovskites: Self-trapping and defects in the bulk and surfaces. *Chem. Mater.* **2020**, *32*, 6916−6924.
(36) Kohn, W.; Sham, L. J. Self-consistent equations including exchange and correlation effects. *Phys. Rev.* **1965**, *140*, A1133.
(37) Hohenberg, P.; Kohn, W. Inhomogeneous electron gas. *Phys. Rev.* **1964**, *136*, B864.
(38) Kresse, G.; Furthmüller, J. Efficient iterative schemes for ab initio total-energy calculations using a plane-wave basis set. *Phys. Rev. B* **1996**, *54*, 11169.
(39) Kresse, G.; Furthmüller, J. Efficiency of ab-initio total energy calculations for metals and semiconductors using a plane-wave basis set. *Comput. Mater. Sci.* **1996**, *6*, 15−50.
(40) Kresse, G.; Joubert, D. From ultrasoft pseudopotentials to the projector augmented-wave method. *Phys. Rev. B* **1999**, *59*, 1758.
(41) Perdew, J. P.; Ruzsinszky, A.; Csonka, G. I.; Vydrov, O. A.; Scuseria, G. E.; Constantin, L. A.; Zhou, X.; Burke, K. Restoring the density-gradient expansion for exchange in solids and surfaces. *Phys. Rev. Lett.* **2008**, *100*, 136406.
(42) Kumagai, Y.; Oba, F. Electrostatics-based finite-size corrections for first-principles point defect calculations. *Phys. Rev. B* **2014**, *89*, 195205.

https://doi.org/10.1021/acsenergylett.2c02306
ACS Energy Lett. 2023, 8, 356−360